Available online at www.sciencedirect.com
ScienceDirect
Nuclear Physics B Proceedings Supplement 00 (2014) 1–7
Nuclear Physics B Proceedings Supplement

Studies of the Higgs boson spin and parity using the $\gamma\gamma$, ZZ, and WW decay channels with the CMS detector

Emanuele Di Marco for the CMS collaboration

CERN, CH-1211 Geneva 23, Switzerland

Abstract

Studies of the Higgs boson spin and parity are presented using data samples corresponding to the $\gamma\gamma$, ZZ, and WW decay channels. The analyses are based on pp collision data collected at centre-of-mass energies of 7 and 8 TeV, corresponding to integrated luminosities of approximately 5 fb^{-1} and 20 fb^{-1}, respectively. The data are compared to the expectations for the standard model Higgs boson, and for several alternative models.

Keywords:

1. Introduction

The observation of a new boson [1, 2] with a mass around 125 GeV and properties consistent with the standard model (SM) Higgs boson was reported by the ATLAS and CMS Collaborations in 2012. The discovery was followed by an extensive set of measurements of its properties to determine if they follow the SM predictions or if there are indications for physics beyond the SM (BSM). The decays of this boson into two electroweak (EW) gauge bosons, $\text{H} \to \text{ZZ} \to 4\ell$, $\text{H} \to \text{WW} \to \ell\nu\ell\nu$, $\text{H} \to \gamma\gamma$, can provide information on the consistency of its spin-parity with the hypothesis of a spin-zero scalar SM Higgs boson.

In this conference I reported the results on the Higgs boson spin-parity properties and tensor structure interactions with EW gauge bosons using the $\text{H} \to \text{ZZ}$, $\text{Z}\gamma^*$, $\gamma^*\gamma^* \to 4\ell$, $\text{H} \to \text{WW} \to \ell\nu\ell\nu$, with $\ell = \text{e}^{\pm}, \mu^{\pm}$, and $\text{H} \to \gamma\gamma$ decay modes. The results are presented in terms of constraints on the anomalous coupling contributions to the HVV interactions for the spin-zero assumption, and hypothesis testing of exotic spin-one and spin-two states. By using the $\text{H} \to \gamma\gamma$ decay channel, the exotic spin-two scenario can be further constrained. For the studies presented, the full Run1 LHC data sample collected by CMS experiment [3] at centre-of-mass energies of 7 and 8 TeV is used.

2. Phenomenology of anomalous HVV interactions

For the studies presented, the formalism of the scattering amplitude is used to describe the interactions of a boson H with a pair of vector bosons V_1 and V_2.

2.1. Spin-zero resonance

For a spin-zero boson H and two spin-one gauge bosons VV, such as ZZ, $\text{Z}\gamma$, $\gamma\gamma$, WW, or gg, the scattering amplitude presents three invariant tensor terms with coupling complex constants a_i^{VV} which in general can depend on the Lorentz invariant four-momenta of V_1 and V_2 squared, $q^2_{\text{V}_1}$ and $q^2_{\text{V}_2}$. In the following, the terms up to q^2_{V} are kept in the expansion under the assumption of small contributions from anomalous couplings

$$A(\text{HVV}) \sim \left[a_1^{\text{VV}} + \frac{\kappa_1^{\text{VV}} q^2_{\text{V}_1} + \kappa_2^{\text{VV}} q^2_{\text{V}_2}}{\left(\Lambda_1^{\text{VV}}\right)^2}\right] m^2_{\text{V}_1} \epsilon^*_{\text{V}_1} \epsilon^*_{\text{V}_2} \quad (1)$$
$$+ a_2^{\text{VV}} f^{*(1)}_{\mu\nu} f^{*(2),\mu\nu} + a_3^{\text{VV}} f^{*(1)}_{\mu\nu} \tilde{f}^{*(2),\mu\nu},$$

where $f^{(i)\mu\nu} = \epsilon^{\mu}_{\text{V}i} q^{\nu}_{\text{V}i} - \epsilon^{\nu}_{\text{V}i} q^{\mu}_{\text{V}i}$ is the field strength tensor of a gauge boson with momentum $q_{\text{V}i}$ and polarization vector $\epsilon_{\text{V}i}$, $\tilde{f}^{(i)}_{\mu\nu} = \frac{1}{2}\epsilon_{\mu\nu\rho\sigma} f^{(i),\rho\sigma}$ is the dual field strength

tensor, the superscript * designates a complex conjugate, m_{V1} is the pole mass of the vector boson Z or W, and Λ_1 is the scale of BSM physics and is a free parameter of the model [4]. The tree-level SM-like contribution corresponds to $a_1^{\mathrm{ZZ}} \neq 0$ and $a_1^{\mathrm{WW}} \neq 0$, while there is no tree-level coupling to massless gauge bosons, that is $a_1^{\mathrm{VV}} = 0$ for $\mathrm{Z}\gamma, \gamma\gamma$, and gg. The other terms in the SM can be generated through loop effects, and are expected to be small to be observed with the current LHC dataset, thus they are considered as anomalous couplings.

The parity-conserving interaction of a pseudoscalar (CP-odd state) corresponds to the a_3^{VV} terms, while the other terms describe the parity-conserving interaction of a scalar (CP-even state). The a_3^{VV} terms appear in the SM only at a three-loop level and receive a small contribution. The a_2^{VV} and Λ_1^{VV} terms appear in loop-induced processes and also give small contributions $O(10^{-3} - 10^{-2})$.

Contributions from BSM particles can change both the magnitude and the phases of these couplings, given their non-trivial dependence on the Lorentz invariant quantities. When the particles in the loops responsible for these couplings are heavy in comparison to the Higgs boson mass, the couplings are real. The scenarios are parameterized in terms of the effective fractional cross sections and their phases with respect to the two dominant tree-level couplings a_1 and a_1^{WW} in the $\mathrm{H} \to \mathrm{VV} \to 4\ell$ and $\mathrm{H} \to \mathrm{WW} \to \ell\nu\ell\nu$ processes, respectively: $(f_{\Lambda 1}, \phi_{\Lambda 1})$, $(f_{a2}, \phi_{a2} = \arg\left(\frac{a_2}{a_1}\right))$, $(f_{a3}, \phi_{a3} = \arg\left(\frac{a_3}{a_1}\right))$. The couplings of the Higgs boson to $\mathrm{Z}\gamma$ and $\gamma\gamma$ are also accessible in these decays and can be measured with the same techniques in the $\mathrm{H} \to 4\ell$ decays, but with the current LHC dataset they are much better constrained via the decays of the on-shell gauge bosons.

The couplings in the $\mathrm{H} \to \mathrm{ZZ} \to 4\ell$ and $\mathrm{H} \to \mathrm{WW} \to \ell\nu\ell\nu$ decay channels can be related with functions of two free parameters. If f_{ai} is the fraction in the HZZ coupling, then the other parameter can be expressed in terms of the ratio of the anomalous couplings of the two channels:

$$r_{ai} = \frac{a_i^{\mathrm{WW}}/a_1^{\mathrm{WW}}}{a_i/a_1}\,, \quad \text{or} \quad R_{ai} = \frac{r_{ai}|r_{ai}|}{1 + r_{ai}^2}\,. \tag{2}$$

A more complete description of the phenomenology of HVV anomalous interactions can be found in Ref.[5].

2.2. Exotic spin-one and spin-two resonance

A spin-one resonance cannot decay into $\gamma\gamma$ final state because of the Landau-Yang theorem. We anyway tested this hypothesis for the ZZ and WW channels, assuming the existence of two states that decay in different modes. We test the spin-two hypothesis for all the three channels. The scattering amplitude of the exotic boson with spin one ($X_{J=1}$) consists of two independent terms, which can be written as

$$A(\mathrm{X}_{J=1}\mathrm{VV}) \sim b_1^{\mathrm{VV}}\left[(\epsilon_{\mathrm{V1}}^* q)\,(\epsilon_{\mathrm{V2}}^* \epsilon_{\mathrm{X}}) + (\epsilon_{\mathrm{V2}}^* q)\,(\epsilon_{\mathrm{V1}}^* \epsilon_{\mathrm{X}})\right] + b_2^{\mathrm{VV}} \epsilon_{\alpha\mu\nu\beta} \epsilon_{\mathrm{X}}^{\alpha} \epsilon_{\mathrm{V1}}^{*\mu} \epsilon_{\mathrm{V2}}^{*\nu} \tilde{q}^{\beta}\,, \tag{3}$$

where ϵ_{X} is the polarization vector of the boson X with spin one, $q = q_{\mathrm{V1}} + q_{\mathrm{V2}}$ and $\tilde{q} = q_{\mathrm{V1}} - q_{\mathrm{V2}}$ [6]. Here the $b_1^{\mathrm{VV}} \neq 0$ coupling corresponds to a vector particle, while the $b_2^{\mathrm{VV}} \neq 0$ coupling corresponds to a pseudovector particle. As in the case of spin-zero resonance, we define a continuous parameter that describes the presence of the corresponding terms b_1^{VV} and b_2^{VV} as an effective fractional cross section f_{b2}^{VV}. The f_{b2}^{VV} parameter is used to test if the data favors the SM Higgs boson scalar hypothesis or some particular mixture of the vector and pseudovector states.

The scattering amplitude for a spin-two boson is more complex and its expression can be found in [5]. It contains ten complex terms, and they are fully tested in this study. In this case we consider both the decays into massive gauge bosons, ZZ or WW, and to two on-shell photons, $\mathrm{X} \to \gamma\gamma$. Both $\mathrm{q\bar{q}}$ production and gluon fusion, spin-two state are considered for the $\mathrm{H} \to 4\ell$ final states. The set of models considered are: 2_m^+, 2_{h2}^+, 2_{h3}^+, 2_h^+, 2_b^+, 2_{h6}^+, 2_{h7}^+, 2_h^-, 2_{h9}^-, 2_{h10}^-. The subscripts m (minimal couplings), h (couplings with higher-dimension operators), and b (bulk) distinguish different scenarios. In the case of the $\gamma\gamma$ decay only the results for a massive graviton-like boson, 2_m^+ are considered.

3. Kinematic observables

The measurements of the spin-parity properties of the Higgs boson make use of the kinematics of the four leptons in the event, for the $\mathrm{H} \to \mathrm{VV}$ decay channels, and of the two photons, for the $\mathrm{H} \to \gamma\gamma$ decay channel. For a spin-zero resonance, there is no correlation between the initial state polarization and the final state kinematic distributions, while for a spin-one or spin-two boson such a correlation introduces non-trivial dependence of the final state on the production mechanism. The techniques to exploit all these informations are described in Ref. [5].

3.1. Kinematics of $\mathrm{H} \to \mathrm{ZZ} \to 4\ell$

The event selection of $\mathrm{H} \to \mathrm{ZZ} \to 4\ell$ candidates is the same as the one used to perform the other measurements in this channel, and reported in [7]. Analogously,

the selected candidates for the $H \to WW \to \ell\nu\ell\nu$ are the same as described in [8].

For the $H \to ZZ \to 4\ell$ decay, events are selected with at least four identified and isolated electrons or muons. The $Z^{(*)} \to \ell^+\ell^-$ candidate is required to be originating from a pair of leptons of the same flavor and opposite charge is required. The $\ell^+\ell^-$ pair with an invariant mass, m_1, nearest to the nominal Z boson mass is retained and is denoted Z_1 if it is in the range $40 \leq m_1 \leq 120\,\text{GeV}$. A second $\ell^+\ell^-$ pair, denoted Z_2, is required to have $12 \leq m_2 \leq 120\,\text{GeV}$. At least one lepton should have $p_T \geq 20\,\text{GeV}$, another one $p_T \geq 10\,\text{GeV}$ and any oppositely charged pair of leptons among the four selected must satisfy $m_{\ell\ell} \geq 4\,\text{GeV}$. For the spin-parity measurements, events are selected in a range around the observed 125.6 GeV resonance, $105.6 \leq m_{4\ell} \leq 140.6\,\text{GeV}$. The dominant background, $q\bar{q} \to ZZ/Z\gamma^*$ and $gg \to ZZ/Z\gamma^*$ processes, are evaluated from simulation, while the reducible non-prompt lepton background, denoted as $Z + X$, is estimated from data control samples with relaxed lepton identification criteria. The event yields are reported in [7].

For this channel, the four-momenta of the $H \to 4\ell$ decay products carry eight independent degrees of freedom, which fully describe the kinematic configuration of a four-lepton system in its center-of-mass frame, except for an arbitrary rotation around the beam axis. These can be conveniently expressed in terms of the five angles $\vec{\Omega} \equiv (\theta^*, \Phi_1, \theta_1, \theta_2, \Phi)$, the invariant masses of the dilepton pairs, m_1 and m_2, and of the four-lepton system, $m_{4\ell}$. We present the distribution of two of these kinematic variables $(m_1, m_{4\ell})$, in data and simulation, in Fig. 1.

One of the approaches pursued in this channels is to parameterize the multidimensional distributions as a function of the parameters of interests, which in this approach are the anomalous couplings [9]. Given the difficulty to populate eight-dimensional distributions for components that cannot be described analytically, like the $gg \to ZZ/Z\gamma^*$ and Z+X processes, this approach is only used for a subset of the measurements for a spin-zero resonance. The analytic parameterization is the product of the differential decay cross section, $d\sigma_{4\ell}$, and the production spectrum, W_{prod}, written as

$$\mathcal{P}(\vec{p}_T, Y, \Phi^*, \vec{x}|\vec{\zeta}) = W_{\text{prod}}(\vec{p}_T, Y, \Phi^*, \hat{s}) \times \frac{d\sigma_{4\ell}(m_{4\ell}, m_1, m_2, \vec{\Omega}|\vec{\zeta})}{dm_1^2 dm_2^2 d\vec{\Omega}}, \quad (4)$$

where $\vec{p}_T$, Y, and Φ^* are the transverse momentum, rapidity, and azimuthal orientation of the four-lepton system, and $\hat{s} = m_{4\ell}^2$ is the center-of-mass energy of the parton-parton system. This probability is converted into detector-level observables through transfer functions, $T(\vec{x}^R|\vec{x}^G)$, describing the detector response to produced leptons. Due to the excellent angular resolution of the CMS tracker, the effect of the resolution on the lepton direction is neglected.

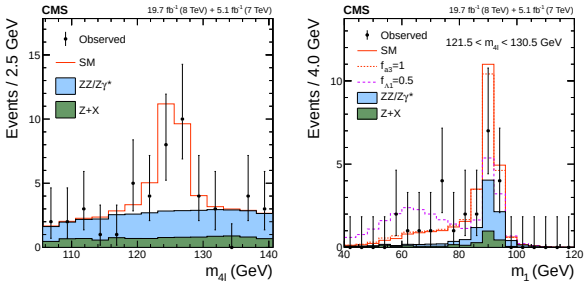

Figure 1: Distributions of two out of the eight kinematic observables used in the $H \to ZZ \to 4\ell$ analysis: $m_{4\ell}$, m_1. Distributions show the observed data (points with error bars), the expectations for the SM background (shaded areas), the SM Higgs boson signal (open areas under the solid histogram), and the alternative spin-zero resonances (open areas under the dashed histograms). The m_1 distribution is presented range of $121.5 < m_{4\ell} < 130.5$ GeV to enhance the signal purity, with the expectations for the SM background, the Higgs boson signal, and some characteristic alternative spin-zero scenarios.

The eight-dimensional analysis can be reduced to a three-dimensional one by storing the full kinematic information in discriminants designed for the separation of either background ($\mathcal{D}_{\text{bkg}}$), the alternative signal components ($\mathcal{D}_{J^P}$), or interference between those components ($\mathcal{D}_{\text{int}}$). The construction of the kinematic discriminants follows the matrix element likelihood approach (MELA package [2, 6]), where the probabilities for an event are calculated using the LO matrix elements as a function of angular and mass observables. The JHUGen matrix elements are used for the signal, gg or $q\bar{q} \to X \to ZZ\,/\,Z\gamma^*\,/\,\gamma^*\gamma^* \to 4\ell$, and MCFM matrix elements for the background, gg or $q\bar{q} \to ZZ\,/\,Z\gamma^*\,/\,\gamma^*\gamma^*\,/\,Z \to 4\ell$. To remove the dependence of the spin-one and spin-two discriminants on the production model, the probability $\mathcal{P}^{\text{kin}}$ is averaged over the two production angles $\cos\theta^*$ and Φ_1, or equivalently the signal matrix element squared is averaged over the polarization of the resonance [4], defining two production-mechanism-independent discriminants, equivalent to the ones for a spin-zero resonance: $\mathcal{D}_{\text{bkg}}^{\text{dec}}$ and $\mathcal{D}_{J^P}^{\text{dec}}$.

3.2. *Kinematics of* $H \to WW \to \ell\nu\ell\nu$

For the $H \to WW \to \ell\nu\ell\nu$ decay, events with exactly one electron and one muon are selected, passing tight

identification criteria to suppress the reducible background from $W+jets$ processes, as described in Ref. [8]. The eμ pair is required to have an invariant mass above 12 GeV, and a p_{T} above 30 GeV. Events are also required to have *projected* $E_{\mathrm{T}}^{\mathrm{miss}}$ above 20 GeV, as defined in Ref. [8]. Signal events with exactly zero or one jet, satisfying $E_{\mathrm{T}} > 30$ GeV and $|\eta| < 4.7$, are dominated by gluon fusion Higgs boson production. The events with two same-flavor leptons or with more than one reconstructed jet are not considered for the spin-parity analysis.

The main backgrounds, the non-resonant WW production and top-quark production ($\mathrm{t\bar{t}}$ and tW processes), are estimated from data. The reducible background arising from misidentified leptons from $W+jets$ processes, is estimated from a data control sample with loosened lepton identification. The normalization of the contribution from the Wγ^* process is also estimated from events in data with three leptons. The residual sub-dominant backgrounds from triboson production (VVV) and WZ and ZZ processes are estimated from simulation. The event yields observed in data and the expectation from the different processes are given in Ref. [8].

As a difference with the H $\rightarrow$ ZZ $\rightarrow 4\ell$ case, only partial reconstruction of the four leptons is possible in this channel, because of the two undetected neutrinos. Two distributions are used in this case, summarizing the kinematics of the two charged leptons and the $E_{\mathrm{T}}^{\mathrm{miss}}$ of the event: the transverse mass of the final state (m_{T}), defined as $m_{\mathrm{T}}^2 = 2p_{\mathrm{T}}^{\ell\ell}E_{\mathrm{T}}^{\mathrm{miss}}(1-\cos\Delta\phi(\ell\ell,\vec{E}_{\mathrm{T}}^{\mathrm{miss}}))$, and the dilepton mass ($m_{\ell\ell}$) which is one of the most discriminating kinematic variables for a Higgs boson with low mass, and it is also correlated to the spin via the azimuthal opening angle between the two leptons. The signal region is defined by $m_{\ell\ell} < 200$ GeV, and $60 \leq m_{\mathrm{T}} \leq 280$ GeV. The distributions of these observables for data, an expected SM Higgs signal and backgrounds are presented in Fig. 2 for events with no reconstructed jets, which constitute the most sensitive category of this analysis.

3.3. *Kinematics of* H $\rightarrow \gamma\gamma$

For this decay channel, the kinematics of the diphoton events are defined by the measurement of the photon energy and position in the electromagnetic calorimeter (ECAL). The selection for the spin-parity analysis is described in Ref. [10]. The cosine of the scattering angle in the Collins–Soper frame, $\cos\theta^*$, is used to discriminate between the spin hypotheses. The angle is defined in the diphoton rest frame as that between the collinear photons and the line that bisects the acute angle between

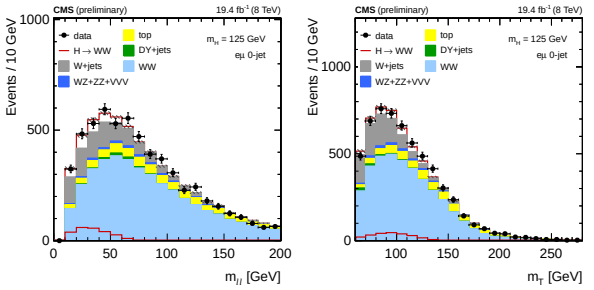

Figure 2: Distributions of the two kinematic observables used in the H $\rightarrow$ WW $\rightarrow \ell\nu\ell\nu$ analysis: $m_{\ell\ell}$, m_{T}. Distributions show the observed data (points with error bars), the expectations for the SM background (filled areas), the SM Higgs boson signal (open areas on top of the solid histogram). The mass of the resonance is taken to be 125 GeV and the SM cross section is used. Events with zero jets are shown.

the colliding protons:

$$\cos\theta^*_{\mathrm{CS}} = 2 \times \frac{E^{\gamma 2}p_z^{\gamma 1} - E^{\gamma 1}p_z^{\gamma 2}}{m_{\gamma\gamma}\sqrt{m_{\gamma\gamma}^2 + (p_{\mathrm{T}}^{\gamma\gamma})^2}}, \quad (5)$$

where $E^{\gamma 1}$ and $E^{\gamma 2}$ are the energies of the leading and subleading photons, $p_z^{\gamma 1}$ and $p_z^{\gamma 2}$ are the z components of their momenta, and $m_{\gamma\gamma}$ and $p_{\mathrm{T}}^{\gamma\gamma}$ are the invariant mass and transverse momentum of the diphoton system. In the rest frame of a spin-0 boson the decay photons are isotropic, and so, before the acceptance requirements, the distribution of $\cos\theta^*_{\mathrm{CS}}$ is uniformly flat under the SM hypothesis. In general, this is not the case for the decay of a spin-2 particle. Within each diphoton class, the events are categorized in five $|\cos\theta^*|$ bins to discriminate between the different spin hypotheses, and split in several categories to enhance the sensitivity.

4. Study of exotic spin-one and spin-two couplings

4.1. H $\rightarrow$ VV $\rightarrow 4\ell$ *final states*

With the H $\rightarrow$ ZZ $\rightarrow 4\ell$ and H $\rightarrow$ WW $\rightarrow \ell\nu\ell\nu$ decay channels the exotic-spin J^P hypotheses for the 125 GeV resonance are tested again the SM one. In addition, mixed spin-one state hypotheses, as well as the comprehensive set of spin-two models listed in Sec. 2 are tested. Finally, the fractional presence of J^P models of a state nearly degenerate in mass with the SM state are tested.

For these studies, template maximum likelihood fits to the kinematic discriminants defined in Sec. 3.1 are used. In the case of H $\rightarrow$ ZZ $\rightarrow 4\ell$ and spin-one, they are ($\mathcal{D}_{\mathrm{bkg}}, \mathcal{D}_{1^-}, \mathcal{D}_{1^+}$). These hypotheses are tested for a

discrete set of values for parameter f_{b2} both for $q\bar{q}$ production and for generic production, using production-independent discriminants. All spin-one tests are consistent with the expectation for the SM Higgs boson. While the decay-only analysis uses less information and is expected to provide weaker constraints, the fluctuations in the observed data lead to stronger constraints for spin-one models. The least restrictive result corresponds to the 1^+ model in the $q\bar{q}$ production test with a CL_s value of 0.031%. Any arbitrary spin-one model for the resonance observed in the $X \to ZZ \to 4\ell$ decay mode with any mixture of parity-even and parity-odd interactions and any production mechanism is excluded at a CL of 99.97% or higher. A summary is shown in Fig. 3 (left).

In the case of $H \to WW \to \ell\nu\ell\nu$, the average separation between the SM Higgs boson and each alternative spin-1 hypothesis is larger than one standard deviation. The alternative spin-1 hypotheses are disfavored with CLs values of 3.9% for 1^-, 14.0% for 1^+, and 8.7% for 1_{mix}. The distribution of the test statistic and the observed value for the case of 1^- against SM is shown in Fig. 3 (right).

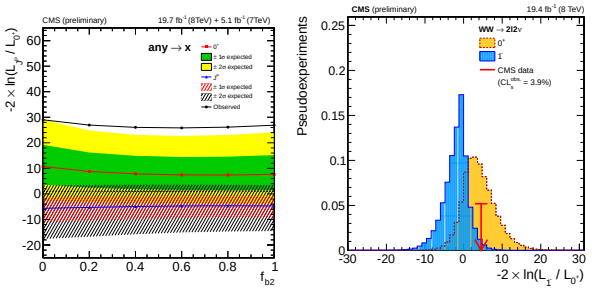

Figure 3: Left: the expected and observed distributions of median test-statistic q for alternative mixed spin-one hypotheses, as a function of f_{b2}, for $H \to ZZ \to 4\ell$, production-independent test. The green and yellow filled bands represent the 1σ and 2σ around the median expected value for the SM Higgs boson hypothesis. The red and black dashed bands represent the 1σ and 2σ around the median expected value for the mixed spin-one hypotheses. Right: Distributions of $-2ln(L_{1^-}/L_{0^+_m})$, combining the 0-jet and 1-jet categories, for the $H \to WW \to \ell\nu\ell\nu$, channel with $q\bar{q}$ production, pure 1^- state. The observed value is indicated by the red arrow.

The hypothesis test of SM Higgs boson against the spin-two resonance is performed for ten models and three scenarios: gg, $q\bar{q}$ production, and using only decay information in the $H \to ZZ \to 4\ell$ decay channel. Interference between the different amplitude components is not considered in this case. The data disfavor all tested spin-two hypotheses in favor of the SM hypothesis 0^+ with $1-CL_s$ values larger than 99% CL in the case of analysis of decay-only observables. There are non-zero correlations between the best-fit values obtained for the various alternate hypotheses. Measurements are also performed for two non-interfering states, indicating no evidence for the presence of a BSM fraction. Fig. 4 (left) shows the distribution of the test statistic q for one of these tests (2^+_{h2}).

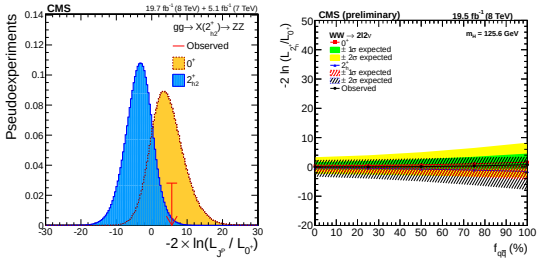

Figure 4: Left: Distributions of the test statistic $q = -2\ln(\mathcal{L}_{J^P}/\mathcal{L}_{0^+})$ for the $J^P = 2^+_{h2}$ hypothesis of $gg \to X(2^+_{h2}) \to ZZ$ tested against the SM Higgs boson hypothesis (0^+). The expectation for the SM Higgs boson is represented by the yellow histogram on the right and the alternative J^P hypothesis by the blue histogram on the left. The red arrow indicates the observed q value. Right: Observed and expected median test statistic for the 0^+ and J = 2 hypotheses, as a function of the $f_{q\bar{q}}$ fraction for the $J^P = 2^+_{h2}$ in the $H \to WW \to \ell\nu\ell\nu$ decay mode.

The results of the hypothesis testing for the spin-one and spin-two hypotheses obtained by considering the $X \to ZZ \to 4\ell$ and $X \to WW \to \ell\nu\ell\nu$ decay channels can be combined, with the assumption that the same tensor structure for the interactions appears in both XZZ and XWW couplings. In case of the spin-one studies, we have tested the models in which the new boson is produced in the $q\bar{q}$ process. In case of the spin-two studies, we have tested the models in which the new boson is allowed to be produced in both the gg and $q\bar{q}$ processes. We have performed these tests for several choices of the ratio of the two production rates $f_{q\bar{q}}$. The analysis which uses information from the $H \to ZZ \to 4\ell$ decay channel is performed in an production-independent way. The analysis in the $H \to WW \to \ell\nu\ell\nu$ decay channel tests for several choices of the ratio of the $f_{q\bar{q}}$ ratio explicitly. The expected separations from the test statistic distributions for all the considered models are summarized in Figure 5. The data disfavor all tested spin-one and spin-two hypotheses in favor of SM hypothesis 0^+ with CL_s value larger then 99.9% CL. Each of these exclusions is tested and reported independently of the other hypotheses, but one should note that there are correlations between the various alternate hypotheses.

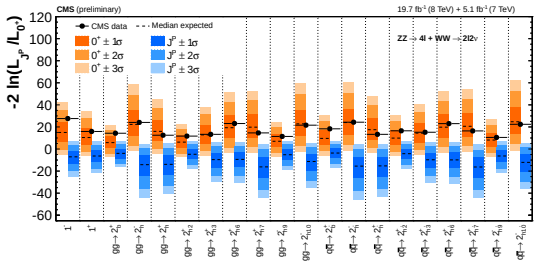

Figure 5: Summary of the expected and observed values for the test-statistic q distributions for the alternative spin-one and spin-two hypotheses tested with respect to the SM Higgs boson, based on the combined analysis in $H \to ZZ \to 4\ell$ and $H \to ZZ \to 4\ell$ decay channels. The orange (blue) bands represent the 1σ, 2σ, and 3σ around the median expected value for the SM Higgs boson hypothesis (alternative hypothesis). The black point represents the observed value.

4.2. $H \to \gamma\gamma$ *final state*

Figure 6 (left) shows the distribution of the expected signal strength, μ, relative to the SM expectation in the five bins of $|\cos\theta^*_{CS}|$ for the SM, and for two 2^+_m models: where the 2^+_m resonance is produced entirely by gluon-fusion (gg), and where it is produced entirely by quark-antiquark annihilation ($q\bar{q}$). The hypothesis of SM Higgs boson is tested against two alternative models of a 2^+_m resonance produced entirely by either gluon-fusion, or entirely by quark-antiquark annihilation, or by three intermediate mixtures of gg and $q\bar{q}$ spin-2 production, with a fraction of cross section $f_{q\bar{q}}$. Figure 6 (right) shows the values of the test statistic as a function of $f_{q\bar{q}}$. The hypothesis of the signal being 2^+_m is disfavored for all values of $f_{q\bar{q}}$ tested.

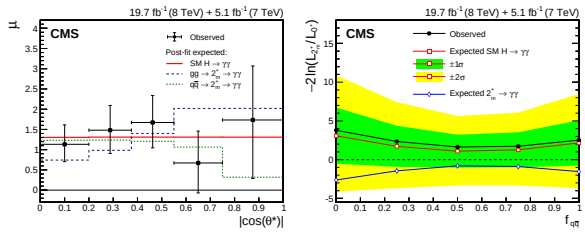

Figure 6: Top: Signal strength in five bins of $|\cos\theta^*_{CS}|$ expected for SM, for 2^+_m produced by gg, and for 2^+_m produced by $q\bar{q}$. The signal strength observed in the data is shown by the black points. Right: Test statistic for pseudo-experiments generated under the SM hypothesis (open squares) and the 2^+_m, hypothesis (open diamonds), as a function of the $f_{q\bar{q}}$ fraction. The observed distribution in the data is shown by the black points.

5. Study of spin-zero HVV couplings

Since an extensive set of exotic resonances have been excluded, measurements are presented of the anomalous coupling for a spin-zero boson decaying into two EW massive gauge bosons (ZZ or WW). The analysis consider three sets of measurements:

1. Constraints on the presence of only one anomalous term in the HVV amplitude of Eq. (2), where the couplings are considered to be real, i.e. $\phi_{ai} = 0$ or π, where ϕ_{ai} generically refers to the phase of the coupling in question, such as $\phi_{\Lambda 1}$, ϕ_{a2}, or ϕ_{a3}. These measurements show no evidence of anomalous couplings. The measurement of the same quantities can be also performed by allowing the coupling to be generically complex, by leaving its phase completely unconstrained. Also these measurement, though with smaller sensitivity, show consistency with the SM expectation.
2. Simultaneous measurements of more than one-anomalous coupling. One possibility is fitting one parameter and leaving another one to be unconstrained, in the full allowed parameter space, with $0 \le f_{ai} \le 1$, in the hypothesis of real couplings. This tests the possible simultaneous presence of more than one anomalous contribution to the amplitude of Eq. (2), without assumptions on one of them. Results are consistent with SM-only amplitude: some two-dimensional scans of the likelihood in the case of real phases are shown in Fig. 7 (top). All other parameters are constrained to be the SM ones. The measurements of f_{a2} and f_{a3} are also performed with the 8-dimensional likelihood, yielding to a consistent result.
3. The same simultaneous measurements can be performed in the case of generic phases, resulting in weaker constraints, but with fewer assumptions. Likelihood scans for three pairs of couplings with generic phases are shown in Fig. 7 (bottom).

The same set of measurements, presented for the $H \to ZZ \to 4\ell$, can be performed in the $H \to WW \to \ell\nu\ell\nu$, though with reduced sensitivity, due to the fewer kinematic observables available, and finally combined together. For the latter, only real couplings, $\phi^{WW}_{ai} = 0$ or π, are considered. The combination can be performed in two scenarios, assuming custodial symmetry ($a^{WW}_1 = a_1$), or not assuming any ratio between the two channels. The relationships between the yield of $H \to ZZ \to 4\ell$ and $H \to WW \to \ell\nu\ell\nu$ yields to stronger constraints on the anomalous couplings. The likelihood scan for a particular value of $R_{ai} = 0.5$ ($r_{ai} = 1$) is shown

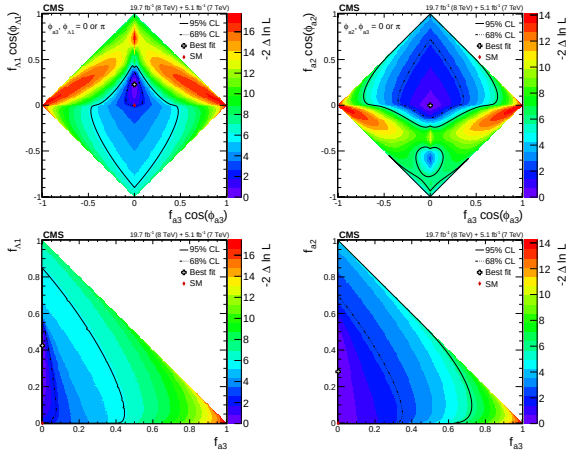

Figure 7: Observed likelihood scans using the template method for pairs of effective fractions, $f_{\Lambda 1}$ vs. f_{a3} (left), and f_{a2} vs. f_{a3} (right) describing HZZ interactions. The top row shows the results where the studied couplings are constrained to be real and all other couplings are fixed to the SM predictions. The bottom row shows the results when the phases of the anomalous couplings are left unconstrained.

in Fig. 8, where the stronger constraint from the yield relationship between the two channels is visible. When the custodial symmetry is assumed, an even stronger constraint arise, strongly disfavoring the hypothesis of $f_{a2} = \pm 1$.

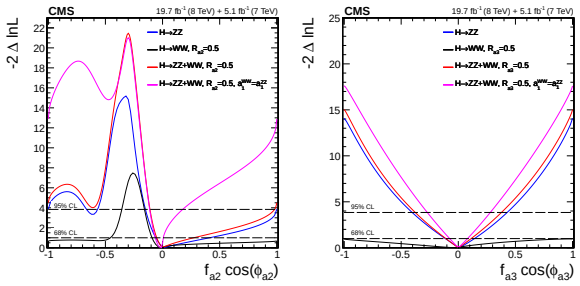

Figure 8: Expected and observed likelihood scans for effective fractions f_{a2} (left), f_{a3} (right). The couplings studied are constrained to be real and all other anomalous couplings are fixed to the SM predictions. The $\cos\phi_{ai}$ term allows a signed quantity where $\cos\phi_{ai} = -1$ or $+1$. The plots show the combined H $\rightarrow$ WW and H $\rightarrow$ ZZ result in terms of the HZZ couplings for $R_{ai} = 0.5$.

Overall, all anomalous HVV couplings are found to be consistent with zero, which is also consistent with the expectation from the SM, where these couplings are expected to be very small, well below the current sensitivity.

6. Conclusions

In this conference the study of a the Higgs boson spin-parity properties have been presented, through its decays into two electroweak gauge bosons: H $\rightarrow$ ZZ, $Z\gamma^*$, $\gamma^*\gamma^* \rightarrow 4\ell$, H $\rightarrow$ WW $\rightarrow \ell\nu\ell\nu$ and H $\rightarrow \gamma\gamma$ decay modes.

For the decays into two EW gauge bosons, Z, W, or γ the tensor structure of its interactions is studied, for the presence of anomalous couplings under spin-zero, -one, and -two hypotheses. The combination of the results in the two decay channels leads to a strong constraint on the anomalous H $\rightarrow$ VV interactions for spin-one (excluded at greater than 99.99% CL) and spin-two (excluded at 99.9% CL for gravity-like minimal couplings and 99% CL or higher for the others).

The measurement of eleven anomalous couplings to the HZZ, HZγ, H$\gamma\gamma$, and HWW interactions under the assumption of a spin-zero Higgs boson yields to results which are all consistent with the expectations for a scalar SM-like Higgs boson.

References

[1] G. Aad, et al., Observation of a new particle in the search for the Standard Model Higgs boson with the ATLAS detector at the LHC, Phys.Lett. B716 (2012) 1–29. arXiv:1207.7214, doi:10.1016/j.physletb.2012.08.020.

[2] S. Chatrchyan, et al., Observation of a new boson at a mass of 125 GeV with the CMS experiment at the LHC, Phys. Lett. B 716 (2012) 30–61. arXiv:1207.7235, doi:10.1016/j.physletb.2012.08.021.

[3] S. Chatrchyan, et al., The CMS experiment at the CERN LHC, JINST 3 (2008) S08004. doi:10.1088/1748-0221/3/08/S08004.

[4] I. Anderson, S. Bolognesi, F. Caola, Y. Gao, A. V. Gritsan, et al., Constraining anomalous HVV interactions at proton and lepton colliders, Phys.Rev. D89 (2014) 035007. arXiv:1309.4819, doi:10.1103/PhysRevD.89.035007.

[5] Constraints on anomalous HVV interactions using H to 4l decays, Tech. Rep. CMS-PAS-HIG-14-014, CERN, Geneva (2014).

[6] Y. Gao, A. V. Gritsan, Z. Guo, K. Melnikov, M. Schulze, et al., Spin determination of single-produced resonances at hadron colliders, Phys.Rev. D81 (2010) 075022. arXiv:1001.3396, doi:10.1103/PhysRevD.81.075022.

[7] S. Chatrchyan, et al., Measurement of the properties of a Higgs boson in the four-lepton final state, Phys.Rev. D89 (2014) 092007. arXiv:1312.5353.

[8] S. Chatrchyan, et al., Measurement of Higgs boson production and properties in the WW decay channel with leptonic final states, JHEP 01 (2014) 096. arXiv:1312.1129, doi:10.1007/JHEP01(2014)096.

[9] Y. Chen, E. Di Marco, J. Lykken, M. Spiropulu, R. Vega-Morales, et al., 8D Likelihood Effective Higgs Couplings Extraction Framework in the Golden ChannelarXiv:1401.2077.

[10] V. Khachatryan, et al., Observation of the diphoton decay of the Higgs boson and measurement of its properties, submitted to *Eur. Phys. J. C* (2014). arXiv:1407.0558.